1st Spanish Fluid Mechanics Conference
Cádiz, June 19-22, 2022

Flow dynamics between two concentric counter-rotating porous cylinders with radial through-flow

Sebastian Altmeyer
Castelldefels School of Telecom and Aerospace Engineering,
*Universitat Politècnica de Catalunya, 08034 Barcelona, Spain**

We investigate the impact of radial mass flux on Taylor-Couette flow [1, 2] in counter-rotating configuration, in which a Hopf bifurcation gives rise to branches of nontrivial solutions. Using direct numerical simulation we elucidate structures, dynamics, stability, and bifurcation behavior in qualitative and quantitative detail as a function of inner Reynolds numbers (Re_i) and radial mass flux (α) spanning a parameter space with a rich variety of solutions. Both radial inflow and strong radial outflow stabilize the system, whereas weak radial outflow has a strong destabilizing effect. We detected the existence of stable ribbons and mixed ribbons with low azimuthal wave number without symmetry restriction. In addition, ribbon solutions and mixed-ribbon solutions can be stable or unstable saddles. Furthermore, in the case of unstable saddles *alternations* between two different symmetrically related saddles generate different heteroclinic cycles. For alternating stationary (in co-moving frame) ribbons the persistence time in one saddle decreases with distance from the onset. The persistence time for the heteroclinic cycle of alternating mixed ribbons shows a more complicated dependence with variation in control parameters and seems to follow an intermittency scenario of type III [3]. Depending on whether the symmetrically related solutions are stationary or time-dependent, the heteroclinic connection can be either of *oscillatory* or *non-oscillatory* type.

SYSTEM

Consider the flow driven in the annular gap between two independently rotating cylinders [1, 2], which can be driven by the inner Reynolds number Re_i (here outer Reynolds number fixed $Re = -125$ for counter-rotating case) and a radial Reynolds number α. Further we use a radius ratio of 0.5 and axial periodic boundary conditions , which are set to $\lambda = 1.6$ equivalent to an axial wavenumber $k = (2\pi/\lambda) = 3.927$.

RESULTS

Figure 1 illustrates the (Re_i, α) parameter space investigated here and provides an overview of the rich variety solutions existing for these control parameters.

Blue and orange lines denote the well-known primary bifurcation thresholds out of the CCF basic state for TVF and SPI, respectively. The modifications in the stability threshold with variation in α has been previously reported [4]. Both radial inflow and strong radial outflow destabilize the system, while a moderate radial outflow (here $0 < \alpha \lesssim 17.6$) stabilizes the system. However, variation of α also alters stability and sequence of primary bifurcating structures itself. For radial inflow and slight radial outflow a stable helical SPI branch bifurcates primary out of CCF, while with increasing α a branch of stable toroidal TVF is the first to appear. The two thresholds meet at the point of higher co-dimension) at $\alpha \approx 3.5$ where the stability is exchanged. For $\alpha \gtrsim 15.2$ TVF bifurcates only unstable. The boundaries and curves above TVF and SPI stability thresholds separate the various regions, labeled A-O, of various flow structures, as listed in the table I including their stability properties (stable (s), alternating (a), unstable (u), non-existent (-)).

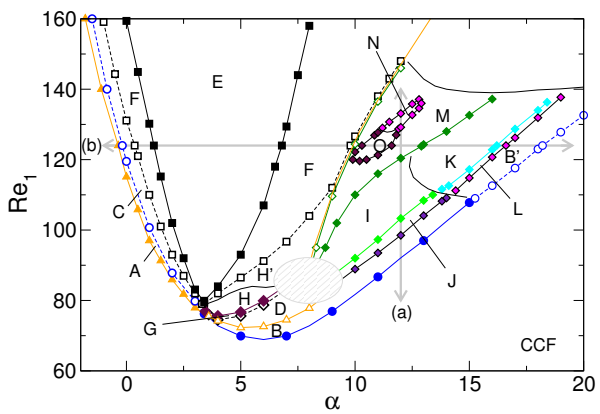

FIG. 1. (Re_i, α) parameter space illustrating various (stable and unstable) solutions. In the hatched area, other perturbations, mainly with larger wavenumbers, destabilize the solutions. See Tab. I for further explanation.

solution	Region														
	A	B[B']	C	D	E	F	G	H[H']	I	J	K	L	M	N	O
TVF	-	s[u]	u	s	s	u	s	s[u]	s	s	u	u	u	u	u
1-wTVF	-	-	-	-	-	s	-	-	-	-	-	-	-	-	-
SPI	s	-	s	u	s	s	u	s	u	u	u	u	u	u	u
wSPI	-	-	-	-	-	-	s	-	-	-	-	-	-	-	-
1-RIB	u	-	u	u	u	u	u	u	s	-	-	-	-	-	-
1-RIB$_{A\leftrightarrow B}$	-	-	-	-	-	-	-	-	-	hc	-	-	-	-	-
1-mRIB$_{A\leftrightarrow B}$	-	-	-	-	-	-	-	-	-	-	-	hc	-	-	-
1-mRIB	-	-	-	-	-	-	-	-	-	-	-	-	s	-	-
1-mRIB^t	-	-	-	-	-	-	-	-	-	-	-	-	-	a	-
1-mRIB$^t_{A\leftrightarrow B}$	-	-	-	-	-	-	-	-	-	-	-	-	-	a	-
L1R1-MCS	-	-	-	-	-	-	-	-	-	-	-	-	-	-	s

TABLE I. Various regions, labeled A-O, as presented in the (Re_i, α) parameter space diagram (Fig. 1) including their stability properties: stable (s), unstable (u), non-existent (-), heteroclinic cycle (hc), alternating (a).

Of special interest are the three regions in which various (m)RIB are stable, unstable, stationary or time-dependent: J: 1-RIB$_{A\leftrightarrow B}$; L: 1-RIB$^t_{A\leftrightarrow B}$; N: 1-mRIB$^t_{A\leftrightarrow B}$;

Figure 2 illustrates the time-periodic change from 1-RIB$_A$ via transitional M0-flow towards 1-RIB$_B$ and vice versa. Both 1-RIB$_A$ and 1-RIB$_B$ have identical kinetic energy, E_{kin}, and Fourier spectra. Within the transi-

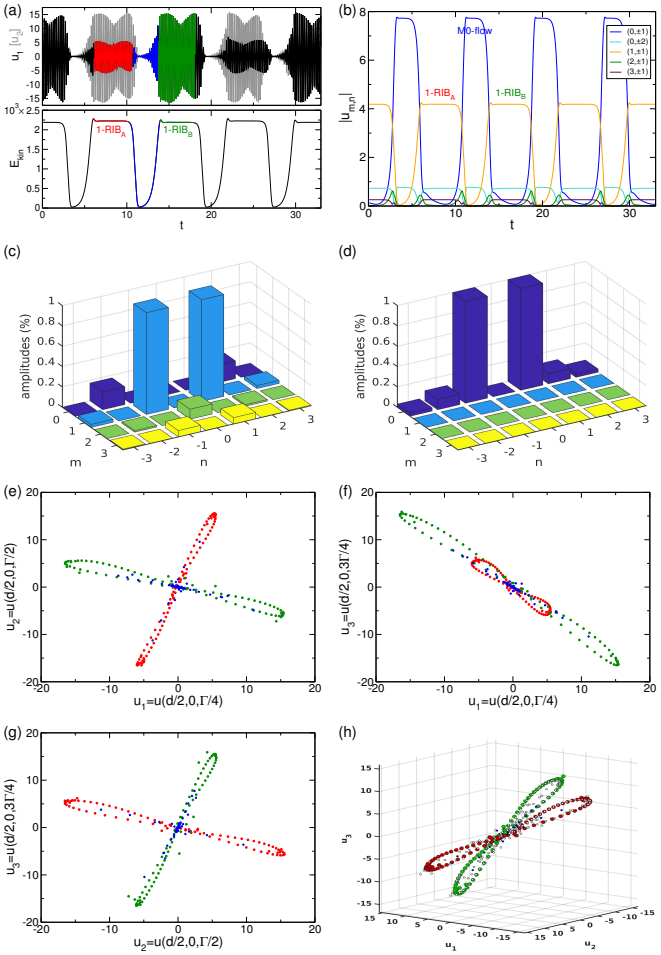

FIG. 2. Visualization of 1-RIB$_{A\leftrightarrow B}$. Shown are dynamics with time of (a) E_{kin} and u_1 [u_2 (light gray)], (b) modes $|u_{m,n}|$; Fourier spectrum (m,n) of (c) 1-RIB$_{A,B}$ and (d) M0-flow, respectively. (e)-(h) Phase portraits spanned by u_1, u_2 and u_3. Control parameters: $\alpha = 12$, $Re_i = 102$.

tional M0-flow E_{kin} almost vanishes. Analogously, the time series of $|u_{m,n}|$ illustrate the elimination of all helical modes $m \geqslant 1$ within the M0-flow, leaving only the toroidal $m = 0$ mode.

However, we emphasize that although the M0-flow only contains $m = 0$ modes, it is crucially different from classical TVF, which consists of a toroidal closed vortex. For our parameters TVF branches super-critically and is stable, co-existing with other solutions (see Fig. and 1). The M0-flow does *not* contain toroidal closed vortices and additionally it is not axisymmetric. Instead, M0-flow retains the symmetries of RIB, which are given by the symmetry group Z_2.

The main dynamics during the transition from 1-RIB$_A$ towards 1-RIB$_B$ can be described as an annihilation and regeneration of a vortex pairs (in the axial direction). First the vortex pairs of 1-RIB$_A$ relocate in its axial position (direction), while moving closer together which results in stretch and compression in the annulus. With increasing time the compression of the vortex pairs eventually results in an annihilation of these vortices, while at the same time two new vortices are generated, which then expand into the annulus. The newly-formed vortex pair is shifted about $\lambda/4$ in axial direction and grows to establish again a temporal solution 1-RIB$_B$. Hereafter the system remains for a time that depends on the parameters in 1-RIB$_B$, before eventually the scenario restarts with a similar back switch to 1-RIB$_A$. The process repeats as long no other external parameters, e.g. α or Re_i are changed.

The phase portraits Fig. 2(e-h) illustrate the connections, i.e. limit cycles, of 1-RIB$_A$ and 1-RIB$_B$. The color coding corresponds to the time series presented in Fig. 2(a,b). The local quantities u_1 and u_2 vs u_3 highlight a perpendicular orientation for 1-RIB$_A$ and 1-RIB$_B$, respectively, resulting in a clover-leaf shape in the corresponding phase portraits (Fig. 2(e-h), with the transitional M0-flow in the core region at the clover-leaf intersection.

CONCLUSIONS

The main results can be summarized as follows.

1. *Stable* ribbons (1-RIBs) at low Reynolds numbers with the smallest (helical) azimuthal wavenumber $m = \pm 1$ [2].
2. *Stable* mixed ribbons (1-mRIBs) as well as *stable* mixed-cross-spirals (MCS)[5] *without* symmetry restrictions. Thereby mRIBs can appear either stationary (1-mRIB) or time-dependent (1-mRIB^t).
3. Heteroclinic cycles between two saddles 1-RIB$_{A\leftrightarrow B}$, 1-mRIB$_{A\leftrightarrow B}$ as well as alternation 1-mRIB$^{(t)}_{A\leftrightarrow B}$.
4. The heteroclinic connection between the two symmetrically related states can be either of *oscillatory type* (for 1-mRIB$^{(t)}_{A\leftrightarrow B}$) or of *non-oscillatory type* (for 1-RIB$_{A\leftrightarrow B}$) [6].
5. For 1-mRIB$^t_{A\leftrightarrow B}$ a more complex intermittency scenario is observed, which seems to be type III intermittency [7].
6. The (Re_i, α) parameter space (Fig. 1) illustrates a rich variety of flow structures.

* sebastian.andreas.altmeyer@upc.edu

[1] G. I. Taylor, *Stability of a viscous liquid contained between two rotating cylinders.* Philos. Trans. R. Soc. London A **223**, 289 (1923).
[2] R. Tagg, *The Couette-Taylor Problem.* Nonlinear Sci. Today **4**, 1 (1994).
[3] S. Altmeyer, *Flow dynamics between two concentric counter-rotating porous cylinders with radial through-flow.* Phys. Rev. Fluids **6**, 124802 (2021)
[4] K. Min and R. M. Lueptow, *Hydrodynamic stability of viscous flow between rotating porous cylinders with radial flow.* Phys. Fluids **6**, 144 (1994).
[5] S. Altmeyer and C. Hoffmann, *Secondary bifurcation of mixed-cross-spirals connecting travelling wave solutions.* New J. Phys. **12**, 113035 (2010).
[6] Y. Bengana and L. Tuckerman, *Spirals and ribbons: frequencies from mean flows and heteroclinic orbits.* Phys. Rev. Fluids **4**, 044402 (2019).
[7] W. M. Macek and M. Strumik, *Hydromagnetic intermittent convection in a magnetized vicous fluid.* Phys. Rev. Lett. **112** (5), 074502 (2014).